Functionalized carbon dots on TiO_2 as stable photoanodes for electrochemical water splitting

A. Ansón-Casaos[1,*], J. Hernández-Ferrer[1], L. Vallan[1], H. Xie[2], M. Lira-Cantú[2], A.M. Benito[1], W.K. Maser[1]

[1]Instituto de Carboquímica, ICB-CSIC, Miguel Luesma Castán 4, 50018 Zaragoza, Spain

[2]Catalan Institute of Nanoscience and Nanotechnology (ICN2), CSIC and Barcelona Institute of Science and Technology (BIST), Building ICN2, Campus UAB, Bellaterra, 08193 Barcelona, Spain

*Corresponding author E-mail: alanson@icb.csic.es

Abstract

Different types of fluorescent carbon nanoparticles, often called carbon dots (CDs), are synthesized by polycondensation and deposited on TiO_2 films to be probed as electron transport layers in organic perovskite photovoltaics and the anode for photoelectrochemical water splitting. Nitrogen CDs, which do not contain oxygen, lead to an increase of around 50 mV in the open circuit voltage of the perovskite cell. All the CD types produce an improved photocurrent in water splitting, particularly CDs that are functionalized with thiol groups and butyl chains. It is demonstrated that the modified electrode is stable under continuous operation for several hours. Other electrochemical characteristics of the electrode, such as the voltammogram shape, onset potentials and open circuit potentials, remain nearly unchanged upon the deposition of CDs. Only the

incident photon to current conversion efficiency improves clearly, extending the absorption range by around 20 nm towards longer wavelengths. This study provides new data about mechanisms and electrode arrangements for improving the performance of n-type semiconductors in photovoltaic cells and photoelectrochemical hydrogen production.

Keywords: Titanium dioxide; carbon nanoparticle; solar energy; renewable hydrogen; sustainability

1. Introduction

Titanium dioxide has been widely studied in advanced oxidation processes, photovoltaics and electrochemical water splitting [1-4]. In particular, TiO_2 films have been utilized as electron transport layers in dye-sensitized and perovskite solar cells [2, 4, 5]. Similar layered configurations, in which TiO_2 behaves as the active phase, are typical in photoelectrochemical (PEC) water oxidation. Intense research efforts are being devoted to improve the performance of these systems [5-7].

The efficiency of TiO_2 photoanodes in electrochemical water splitting has been increased by many strategies, including metal nanoparticle deposition, cationic and anionic doping, and sensitization [1, 8]. In addition, mixtures with carbon materials such as carbon nanotubes [9-12] and graphene [13-16] have been tried. More recently, it has been observed that carbon dots (CDs) on TiO_2 can lead to positive effects in reactions of photoassisted hydrogen generation. Currently, the family of CDs includes many types of fluorescent nanoparticles that are synthesized either by top-down methods, typically from graphite, or bottom-up processes from simple organics such as short chain acids and amines. Many of the CD forms have graphene structures in their

cores, and are usually called graphene quantum dots. Some others do not present conjugated carbon chains, and are sometimes called polymer dots. The photoluminescence properties of CDs are determined by the synthesis method and can be tuned by functionalization with chemical groups that induce charge transfer effects [17].

In the literature, CDs for PEC water splitting have been mostly prepared by electrochemical etching of graphite [18-22] or by hydrothermal synthesis from organic compounds such as ascorbic acid [23], trinitropyrene [24], citric acid [25-27], ethylenediamine [28] and glucose/dicyandiamine [29]. Typically, the CD/TiO_2 composite is treated under hydrothermal conditions to improve the interaction between CDs and nanostructured TiO_2. Alternatively, the CD/TiO_2 photoanode can be prepared by immersion or electrochemical impregnation of the TiO_2 layer in the CD solution [20-22, 26, 27, 30]. The PEC hydrogen generation with CD/TiO_2 photocatalysts has been performed in neutral (e.g. 0.5M Na_2SO_4) or alkaline (1M KOH) electrolytes. Therefore, previous works indicate that CDs improve the TiO_2 activity on PEC water splitting. However, the great number of CD structures and possible electrode configurations suggest that other suitable combinations are still to be found.

It is apparent that both charge transport in the composite solid phase and reactions taking place in the solid-electrolyte interphase are complex and difficult to elucidate. Typically, the proposed mechanisms for the improvement of photocatalytic water splitting on CD/TiO_2 electrodes include sensitization, a fast electron transfer, effects of CD fluorescence and others. Several works have evidenced sensitization from CDs to TiO_2 under visible light, with fast transfer of excited electrons from the HUMO level of the CD to the conduction band of TiO_2 [18, 19, 21, 23, 26-28, 30]. This mechanism for water splitting operates in other CD/semiconductor electrodes such as CD/Fe_2O_3 [31],

CD/ZnO [32] and CD/WO_3 [33]. However, electron transfer from TiO_2 to the CD seems to be also possible, particularly under UV irradiation [19, 23]. Other research works more specifically remark the CD effect of improving charge separation efficiency and decreasing the electron transport resistance [20, 24, 34].

Even though CDs can be prepared by a number of techniques and protocols, all of them have a greatly rich surface chemistry with a variety of functional groups containing oxygen, nitrogen and sulfur. Similarly to other carbon materials, nitrogen and sulfur doping in CDs has been related to the activity as co-catalyst in the cathode for electrochemical hydrogen evolution [35]. In addition, it has been reported that amino groups can active mechanisms of electron transfer to CDs during the photocatalytic hydrogen evolution [36]. In TiO_2 photoanodes, the role of the nitrogen doping level in hydrothermally synthesized CDs has been evidenced on both the photocatalytic hydrogen evolution and PEC water splitting [37]. A positive effect may also result from the co-sensitization of TiO_2 with CDs and Eosin Y dye [38]. However, the functionalization of CDs with specific chemical groups has been seldom explored for photocatalytic and PEC applications, in particular for hydrogen generation and water splitting. In addition, problems with the long term stability of CDs have been detected by several authors [28], which need to be considered for practical application.

In the present work, CDs were prepared by either microwave-assisted or hydrothermal methods, resulting in various structures and compositions. Furthermore, CDs were functionalized with different chemical groups on their surface. The CDs were deposited on TiO_2 electrodes, which were used both in perovskite solar cells and as photoanodes for PEC water splitting. A substantial increase in the photocurrent of PEC water splitting was measured on the photoanode that was modified with chemically functionalized CDs. It was confirmed that the system is stable for several hours of

continuous PEC operation. Finally, novel conclusions on the mechanism of the PEC water splitting were drawn by comparison with results from photovoltaic cells.

2. Experimental

2.1. Synthesis of CDs

Three types of carbon nanoparticles, here labelled as MW-CDs, HS-CDs and But-CDs, are formed by polycondensation between citric acid and ethylenediamine and thus have a common basic polymeric structural unit (Figure 1a). The MW-CDs is synthetized in a microwave system (CEM Discover SP reactor working in the open-batch modality) at high temperatures, while HS-CDs and But-CDs are synthetized in solution at room temperature, employing a coupling agent. Another important difference concerns the functionalization type: MW-CDs are synthesized only with citric acid and ethylenediamine and the resulting polymer structure resembles the one in Figure 1b, where the functional groups are carboxylic acids, amines and alcohols [39]. In the synthesis of HS-CDs and But-CDs, one more step, which is a final addition of a nucleophilic amine, produces an additional functionalization. In this step the carboxylic acids (which are activated towards amines by the coupling agent) react with the added amine (cysteamine for HS-CDs and butyl amine for But-CDs). Therefore carboxylic acids are partially consumed and a new functional group is attached on the polymer structure, i.e. butyl- in But-CDs and thiol in HS-CDs [40]. In addition, primary amines from ethylenediamine and alcohols are still present. The structure of o-PDA-CDs is completely different: the only reagent is *o*-phenylenediamine, which reacts with itself. Most probably the amine reacts with the aromatic ring, resulting in a completely conjugated polyaromatic structure (in contrast, the other CDs are non-conjugated).

For MW-CDs, citric acid monohydrate (2.0 g, 9.5 mmol) was dissolved in ultrapure water (16 mL). Upon addition of ethylenediamine (0.64 mL, 9.5 mmol), the solution was heated through microwave irradiation. The mixture was irradiated to keep the temperature at 140°C for 6 min and then irradiation was stopped. This yielded a yellow, transparent, solid product that was highly soluble in water. The product was dissolved in ultrapure water and dialyzed against ultrapure water (MWCO=0.5–1.0 KDa, 3 days, twice a day). Dry MW-CDs were obtained by freeze-drying (yield in mass of 22 wt%).

For But-CDs, 300 mg of anhydrous citric acid (1.6 mmol, 1 eq.) was dissolved in 4.0 ml of DMF. The solution was cooled in an ice bath and 0.73 ml of diisopropyl carbodiimide (DIC, 3 eq.) were added. Subsequently, 105 µl of ethylenediamine (1 eq.) in 4 ml of water were added and the reaction was stirred for 10 minutes at room temperature, during which the mixture turns its color from slightly yellow to orange. Afterwards 0.62 ml of n-butylamine (4 eq.) dissolved in 4 ml of water were poured into the reaction. The reaction was stirred for 1 hour. The crude was diluted in ultrapure water, filtrated on paper filter and washed with ethyl acetate 2 times and dichloromethane 2 times. Finally the water phase was adjusted to pH=7 with a diluited HCl solution and dialyzed against ultrapure water (MWCO = 0.5-1.0 KDa, 4 days, twice a day). After filtration on a 0.22 µm pore-size filter, the water was removed by freeze-drying, obtaining 250 mg of product.

For HS-CDs, 300 mg of anhydrous citric acid (1.5 mmol, 1 eq.) was dissolved in 4.0 ml of DMF. The solution was cooled in an ice bath and 0.73 ml of diisopropyl carbodiimide (DIC, 3 eq.) were added. Subsequently, 105 µl of ethylenediamine (1 eq.) in 4 ml of water were added and the reaction was stirred for 10 minutes at room temperature, during which the mixture turns its color from slightly yellow to orange. Afterwards 480 mg of cysteamine (4 eq.) dissolved in 4 ml of water were poured into

the reaction. The reaction was stirred for 1 hour. The crude was diluted in ultrapure water, filtrated on paper filter and washed with ethyl acetate 3 times. Finally the water phase was adjusted to pH=7 with a diluited HCl solution and dialyzed against ultrapure water (MWCO = 0.5-1.0 KDa, 4 days, twice a day). After filtration on a 0.22 μm pore-size filter, the water was removed by freeze-drying, obtaining 160 mg of product.

For o-PDA-CDs, *o*-phenylenediamine (0.8 g) was dissolved in water (8 mL) and treated in an autoclave at 200°C for 4 h. Purification was performed by filtration through 3 μm and 0.22 μm filters. The remaining water was removed by vacuum. The solid was redispersed in THF and dried again.

2.2. Electrode preparation

Fluorinated tin oxide (FTO) substrates (Nippon Sheet Glass. 10 Ω/sq) were etched with Zn powder and 4M HCl, next cleaned with Hellmanex®, acetone and ethanol, respectively for 15 min, inside an ultrasonic bath, and immediately blown with dry air. The compact TiO_2 (c-TiO_2) solution was prepared with titanium diisopropoxide bis(acetylacetonate): acetylacetone: ethanol at 0.6: 0.4: 9 volume ratio and sprayed onto FTO substrates at 450ºC. The mesoporous TiO_2 (m-TiO_2) paste was prepared mixing a commercial titanium paste (Dyesol, now Greatcell) with ethanol at 1:6 weight ratio; it was spin-coated onto the c-TiO_2 layer at 5000 rpm for 20 s and then dried at 80ºC for 5 min. The CD suspension (500 μL) was spin-coated onto FTO/c-TiO_2/m-TiO_2 substrates at 3000 rpm for 30 s, and then annealed at 450 °C on a hot plate in air for 30 min.

2.3. Characterization techniques

Elemental analysis (O, C, H, N, S) was performed in a Thermo Flash 1112 analyzer. Fourier-transform infrared (IR) spectroscopy was performed in a Bruker Vertex 70

spectrometer, on powder samples pressed with KBr into pellets. UV/Vis absorption spectra were recorded in a Shimadzu UV-2401 PC spectrophotometer. Photoluminescence excitation and emission spectra were recorded in a Horiba Jobin Yvon Fluoromax-P. All the spectra were recorded at room temperature using a 10 mm path-length quartz cuvette.

Scanning electron microscopy (SEM) was performed in a SEM-EDX Hitachi S-3400 N provided with a Si EDX analyser Röntec XFlash. Micro-Raman spectra were obtained by means of a HORIBA Jobin Yvon Raman spectrometer HR 800UV. The spectra were acquired with a green laser at 532 nm under the 50x objective. X-ray photoelectron spectroscopy (XPS) measurements were taken with an ESCAPlus spectrometer using the Al anode. Contact angle measurements were carried out by the sessile drop method in an Attension Optical Tensiometer by Biolin Scientific.

2.3. Perovskite cell fabrication and assessment

The quadruple cation halide perovskite $Rb_{0.05}Cs_{0.05}MA_{0.15}FA_{0.75}Pb_{1.05}(I_{0.89}Br_{0.11})_3$ was prepared by mixing PbI_2 (1.5 M), $PbBr_2$ (1.5 M), CsI (1.5 M), RbI (1.5 M), MAI and MABr in DMF:DMSO mixed solvent (4:1). The perovskite spin coating process was carried out at 2000 rpm for 10 s, and then 6000 rpm for 30s in a dry air glove box. During the second step of spin coating, 100 μL of chlorobenzene was injected at 15s before ending. Samples were annealed at 100 °C for 1 h on a hot plate for crystallization. The hole transporting layer was prepared by dissolving 0.12 g of spiro-OMeTAD in 1130 μL of chlorobenzene and then doping with 47.3 μL of TBP and 23.5 μL of TFSI (1.8 M in acetonitrile). The spin coating was conducted at 4000 rpm for 20 s. The finished devices were placed inside a dry air box for 12 hours to fully oxidize the

spiro-OMeTAD. Finally, 80 nm of Au was deposited as the front electrode by thermal evaporation.

The solar cells were measured using a 450 W Xenon light source (Oriel) equipped with an arc lamp housing (Newport, Model 66902, 50-500 W). The light intensity was calibrated with a Si photodiode equipped with an infrared cutoff filter (KG3, Schott), and was recorded during each measurement. The I-V curves were measured with a digital source meter (Keithley 2400). The voltage scan rate was 10 mV/s. The cells were masked to get 0.16 cm^2 active area. All the measurements were conducted in air at room temperature.

2.4. PEC water splitting

The PEC measurements were performed in a three electrode cell provided with a quartz window, using an AUTOLAB PGSTAT302N. A graphite rod purchased from CYMIT Quimica was used as the counter electrode. Illumination was carried out using a 150 W Xe arc lamp by LOT-Oriel GmbH, which simulates the solar spectrum in the ultraviolet and visible regions.

A reference electrode of Hg/HgO, 0.1M KOH (E^o = 0.165 V vs. SHE) was utilized for the experiments. A nitrogen purge was utilized to avoid interferences of the oxygen reduction reaction. Experiments were performed in 0.1M NaOH. Three electrochemical tests were performed: cyclic voltammetry, potentiostatic photocurrent and open circuit potential measurements.

For cyclic voltammetry, the scan rate was of 20 $mV \cdot s^{-1}$. Several cycles were performed to detect the possible presence of irreversible phenomena. As a general observation, the fourth cycle was totally reproducible and thus is the one presented here. For voltammetry under irradiation, light was applied continuously during the whole cycle.

For photocurrent measurements under potentiostatic conditions, a bias potential of 0.037 V (vs. Hg/HgO, 0.1M KOH) at pH 13 was applied, which respectively corresponds to the maximum voltage values in the cyclic voltammogram. Intermittent irradiation and dark periods of 15 s were applied during 5 min. For the open circuit potential measurements at zero current, the cell was allowed to stabilize under dark conditions, and then the electrode was illuminated for 1 min. The photopotential (V_{ph}) was calculated as the difference between illumination and dark voltages.

Incident photon to current efficiency (IPCE) was measured under identical conditions to potentiostatic photocurrent experiments using a LOT Oriel monochromator.

3. Results and discussion

3.1. Characterization of CDs

The elemental analysis of the CDs is presented in Figure 2a. The MW-CD nanoparticles contain approximately 45 wt.% of carbon, as well as oxygen and nitrogen as heteroatoms. The HS-CDs show a certain quantity of sulfur, corresponding to thiol groups, together with a decrease in the oxygen with respect to MW-CDs. The But-CDs show an increase in the carbon ratio and a decrease in the oxygen, which support the success of the preparation by functionalization of MW-CDs with butyl chains. The o-PDA-CDs are mostly composed by carbon, nitrogen and hydrogen, but does not contain oxygen.

The IR spectra are presented in Figure 2b. The signals confirm the expected functional groups for the different CD types [41]. The MW-CDs show clear features of alcohol/phenol at around 3400, 3260 and 1440-1390 cm^{-1}, carboxylic acids at 1560 cm^{-1}, and other oxygen and nitrogen groups in the range of 1190-1000 cm^{-1}. The HS-CDs

show features similar to the MW-CDs, while typically the thiol group is hardly detectable by IR spectroscopy. The But-CDs present the features of oxygen and nitrogen groups too; however, methylene bands in the range of 2970-2870 cm^{-1} are particularly relevant, and signals at 1200-1000 cm^{-1} are weak, which is consistent with the presence of butyl chains instead of certain oxygen groups.

Optical properties of CDs are presented in Figure 2c (absorbance) and 2d (fluorescence). Spectra of MW-, HS- and But-CDs show intense light absorption in the UV region ($\lambda < 300$ nm) and an additional maximum at around 350 nm. In o-PDA-CDs, the intense continuous absorption extends to 350 nm, while the additional maximum shifts to around 420 nm. Emission spectra of MW-, HS- and But-CDs show maxima at 446, 434 and 446 nm respectively. The emission band of o-PDA-CDs has two clear contributions with maxima at 499 and around 560 nm.

3.2. Electrode characterization

The characterization of c-TiO_2 / m-TiO_2 + CD electrodes was performed by SEM-EDX (Figure 3), Raman spectroscopy, XPS and contact angle measurements (Figure 4). The EDX analysis covers an electrode area in the range of a mm^2, thus being well representative of the electrode composition. The analysis depth reaches the Sn from the FTO substrate. The reference c-TiO_2 / m-TiO_2 electrode contains adventitious carbon, while all the electrodes with CDs present increased quantities of carbon in its composition. Raman spectra indicate that TiO_2 on the electrodes is mostly in the anatase phase, while it might contain only very small quantities of rutile. The phase composition of TiO_2 does not suffer changes upon the addition of CDs. Similarly, the XPS analysis does not detect substantial changes in the chemical environment of titanium with the deposition of CDs. Contact angle measurements with pure water reveal an increase in

the hydrophobic character of the TiO_2 surface after the deposition of o-PDA-CDs; the other functionalized CDs do not induce changes with respect to the reference TiO_2 electrode.

3.3. Perovskite cells

Figure 5 presents a configuration schematic and the results in perovskite cells. The perovskite active material was infiltrated on the c-TiO_2 / m-TiO_2 + CD region, according to the schematic in Figure 5. Typical j vs. V plots were obtained and the characteristic cell parameters were calculated. The results are in good agreement with previous works under similar cell configurations [42, 43]. Statistically, the photoconversion efficiency (PCE) is kept with the deposition of CDs on the TiO_2 electrode, and remains around 17% (Figure 5c). Similarly, other characteristic parameters (j_{SC}, FF) remain nearly unchanged. Interestingly, the open circuit voltage (V_{OC}) experiences a substantial increase with the deposition of o-PDA-CDs. This change in V_{OC} has to be associated to differential characteristics of o-PDA-CDs. First of all, their composition and structure are different from the other CDs, in particular the high nitrogen ratio and the absence of oxygen. As a consequence, the contact angle of the c-TiO_2 / m-TiO_2 + But-CD surface increases, indicating an increase in the hydrophobic character. Since the perovskite is infiltrated as an organic solution in the cell, the hydrophobic character might improve the structural characteristics of perovskite crystals. Secondly, the optical absorbance and photoluminescence properties of the o-PDA-CDs are also substantially different, suggesting particular optical and electronic responses. Recent works on perovskite cells have underlined the positive effect of N-doping in graphene quantum dots to improve their properties against humidity, temperature stress and UV irradiation, as well as a hole transport material [44,

45]. In the present work, it is further observed that CDs containing only nitrogen as a heteroatom, but not oxygen, might be superior that typical N-doped quantum dots.

3.4. PEC water splitting

The results of PEC water oxidation are presented in Figures 6-9. The cyclic voltammetry experiment (Figure 6) on the reference c-TiO_2 / m-TiO_2 electrode shows an anodic photocurrent at E > -1 V (vs. Hg/HgO). This photocurrent has to be strictly related to water oxidation with evolution of O_2 in the working electrode, and thus to H_2 evolution in the counter electrode. The deposition of CDs on the reference c-TiO_2 / m-TiO_2 electrode provides an increase in the photocurrent, particularly in the case of But-CDs. However, other voltammetry characteristics, such as the onset potentials at around -1 V (vs. Hg/HgO) and the presence of Wilson states in the cathodic scan at around -1.1 V (vs. Hg/HgO) [10] are not modified by the CDs, indicating that the general mechanism of the reaction is unchanged.

Amperometric experiments at E > -1 V were conducted to evaluate the kinetics of the system response and the long term stability (Figure 7). It is confirmed that the deposition of But-CDs substantially improves the photocurrent without altering the speed in the response. In addition, the c-TiO_2 / m-TiO_2 + But-CD system is stable for more than 4 h under continuous operation in PEC water splitting. All the CD-modified electrodes, at equivalent working potentials of E > -1 V (vs. Hg/HgO), produce higher photocurrents than the reference TiO_2 electrode. However, the photopotential, calculated from open circuit voltages (j = 0), does not show substantial changes (Figure 8). This fact, in agreement with observations on cyclic voltammograms, indicates that no substantial changes are introduced by CDs in the reaction mechanism on the TiO_2

electrode. In addition, this agrees with the results in perovskite cells, which indicate few changes in the electron transport properties.

Figure 9 shows the conversion efficiency as a function of the incident irradiation wavelength. The outcomes prove that the CD-modified electrode has a higher efficiency than the reference TiO_2 electrode at larger irradiation wavelengths. The light absorption range is extended by approximately 20 nm. Therefore, the increase in the photocurrent can be associated with a contribution of a light harvesting path through the CD (Figure 10). Both the TiO_2 and CDs are simultaneously working as semiconductors, absorbing photons and pumping excited photoelectrons, while the photoholes react oxidizing water. The CDs provide an equivalent bandgap somewhat narrower than TiO_2. However, all the photoelectron paths seem to be flowing through TiO_2, since onset potentials and photopotentials for the process are not modified. As a consequence, it is deduced that the LUMO level of the CD is located at a higher energy than the lowest active level of the TiO_2 conduction band. Functional groups on the CD might modulate the energy levels to achieve the most suitable interaction with TiO_2.

Conclusions

Various types of fluorescent CDs with different functional groups were synthesized and deposited on thin film c-TiO_2 / m-TiO_2 electrodes. A comparison was performed using analogous electrodes as anode components in perovskite photovoltaic cells and as active photoanodes in PEC water splitting. In perovskite cells, an increase in V_{OC} occurs upon deposition of o-PDA-CDs, which has to be associated to their particular properties: a high nitrogen ratio, absence of oxygen, increased hydrophobic character and different optical behavior. The PEC water oxidation, in terms of photocurrent, improves upon CD deposition, and the increment depends on functionalization. The highest photocurrents

were measured on c-TiO_2 / m-TiO_2 + But-CD electrodes, which are proved to be stable under continuous operation for several hours. All the PEC experiments, and particularly the IPCE, demonstrate that CDs work as sensitizers of TiO_2. The CDs act themselves as semiconductors that increase the optical absorption range by approximately 20 nm, thus increasing the current flow through TiO_2.

Acknowledgements

This work has been funded by the Spanish MINEICO under the project ENE 2016-79282-C5-1-R (AEI/FEDER, UE), the Government of Aragón (Grupo reconocido T03-17R) and associated EU Regional Development Funds (DGA/FEDER, UE). Special thanks are directed to the Analysis Service at Instituto de Carboquímica ICB-CSIC.

References

[1] M. Ni, M. Leung, D. Leung, K. Sumathy, A review and recent developments in photocatalytic water-splitting using TiO2 for hydrogen production, Renewable & Sustainable Energy Reviews 11(3) (2007) 401-425.
[2] M. Pagliaro, G. Palmisano, R. Ciriminna, V. Loddo, Nanochemistry aspects of titania in dye-sensitized solar cells, Energy & Environmental Science 2(8) (2009) 838-844.
[3] J. Schneider, M. Matsuoka, M. Takeuchi, J. Zhang, Y. Horiuchi, M. Anpo, D. Bahnemann, Understanding TiO2 Photocatalysis: Mechanisms and Materials, Chemical Reviews 114(19) (2014) 9919-9986.
[4] Y. Bai, I. Mora-Sero, F. De Angelis, J. Bisquert, P. Wang, Titanium Dioxide Nanomaterials for Photovoltaic Applications, Chemical Reviews 114(19) (2014) 10095-10130.
[5] C. Zhen, T. Wu, R. Chen, L. Wang, G. Liu, H. Cheng, Strategies for Modifying TiO2 Based Electron Transport Layers to Boost Perovskite Solar Cells, Acs Sustainable Chemistry & Engineering 7(5) (2019) 4586-4618.
[6] R. Singh, S. Dutta, A review on H-2 production through photocatalytic reactions using TiO2/TiO2-assisted catalysts, Fuel 220 (2018) 607-620.
[7] J. Jian, G. Jiang, R. van de Krol, B. Wei, H. Wang, Recent advances in rational engineering of multinary semiconductors for photoelectrochemical hydrogen generation, Nano Energy 51 (2018) 457-480.
[8] B. Cecconi, N. Manfredi, T. Montini, P. Fornasiero, A. Abbotto, Dye-Sensitized Solar Hydrogen Production: The Emerging Role of Metal-Free Organic Sensitizers, European Journal of Organic Chemistry (31) (2016) 5194-5215.

[9] J. Yu, T. Ma, S. Liu, Enhanced photocatalytic activity of mesoporous TiO2 aggregates by embedding carbon nanotubes as electron-transfer channel, Physical Chemistry Chemical Physics 13(8) (2011) 3491-3501.
[10] A. Anson-Casaos, J. Hernandez-Ferrer, C. Rubio-Munoz, A. Santidrian, M. Teresa Martinez, A.M. Benito, W.K. Maser, Electron Trap States and Photopotential of Nanocrystalline Titanium Dioxide Electrodes Filled with Single-Walled Carbon Nanotubes, Chemelectrochem 4(9) (2017) 2300-2307.
[11] B. Ng, L. Putri, L. Tan, P. Pasbakhsh, S. Chai, All-solid-state Z-scheme photocatalyst with carbon nanotubes as an electron mediator for hydrogen evolution under simulated solar light, Chemical Engineering Journal 316 (2017) 41-49.
[12] J. Olowoyo, M. Kumar, S. Jain, J. Babalola, A. Vorontsov, U. Kumar, Insights into Reinforced Photocatalytic Activity of the CNT-TiO2 Nanocomposite for CO2 Reduction and Water Splitting, Journal of Physical Chemistry C 123(1) (2019) 367-378.
[13] H. Kim, G. Moon, D. Monllor-Satoca, Y. Park, W. Choi, Solar Photoconversion Using Graphene/TiO2 Composites: Nanographene Shell on TiO2 Core versus TiO2 Nanoparticles on Graphene Sheet, Journal of Physical Chemistry C 116(1) (2012) 1535-1543.
[14] X. Zhang, Y. Sun, X. Cui, Z. Jiang, A green and facile synthesis of TiO2/graphene nanocomposites and their photocatalytic activity for hydrogen evolution, International Journal of Hydrogen Energy 37(1) (2012) 811-815.
[15] X. Zhang, B. Zhang, D. Huang, H. Yuan, M. Wang, Y. Shen, TiO2 nanotubes modified with electrochemically reduced graphene oxide for photoelectrochemical water splitting, Carbon 80 (2014) 591-598.
[16] A. Morais, C. Longo, J. Araujo, M. Barroso, J. Durrant, A. Nogueira, Nanocrystalline anatase TiO2/reduced graphene oxide composite films as photoanodes for photoelectrochemical water splitting studies: the role of reduced graphene oxide, Physical Chemistry Chemical Physics 18(4) (2016) 2608-2616.
[17] S. Jin, D. Kim, G. Jun, S. Hong, S. Jeon, Tuning the Photoluminescence of Graphene Quantum Dots through the Charge Transfer Effect of Functional Groups, Acs Nano 7(2) (2013) 1239-1245.
[18] X. Zhang, F. Wang, H. Huang, H. Li, X. Han, Y. Liu, Z. Kang, Carbon quantum dot sensitized TiO2 nanotube arrays for photoelectrochemical hydrogen generation under visible light, Nanoscale 5(6) (2013) 2274-2278.
[19] H. Yu, Y. Zhao, C. Zhou, L. Shang, Y. Peng, Y. Cao, L. Wu, C. Tung, T. Zhang, Carbon quantum dots/TiO2 composites for efficient photocatalytic hydrogen evolution, Journal of Materials Chemistry a 2(10) (2014) 3344-3351.
[20] L. Sang, J. Lin, Y. Zhao, Preparation of carbon dots/TiO2 electrodes and their photoelectrochemical activities for water splitting, International Journal of Hydrogen Energy 42(17) (2017) 12122-12132.
[21] Q. Wang, J. Huang, H. Sun, K. Zhang, Y. Lai, Uniform carbon dots@TiO2 nanotube arrays with full spectrum wavelength light activation for efficient dye degradation and overall water splitting, Nanoscale 9(41) (2017) 16046-16058.
[22] Y. Zhang, H. Tian, G. Zhao, Enhanced Visible-Light Photoelectrocatalytic Activity of {001}TiO2 Electrodes Assisted with Carbon Quantum Dots, Chemelectrochem 2(11) (2015) 1728-1734.
[23] J. Wang, M. Gao, G. Ho, Bidentate-complex-derived TiO2/carbon dot photocatalysts: in situ synthesis, versatile heterostructures, and enhanced H-2 evolution, Journal of Materials Chemistry a 2(16) (2014) 5703-5709.

[24] S. Yu, Y. Zhong, B. Yu, S. Cai, L. Wu, Y. Zhou, Graphene quantum dots to enhance the photocatalytic hydrogen evolution efficiency of anatase TiO2 with exposed {001} facet, Physical Chemistry Chemical Physics 18(30) (2016) 20338-20344.
[25] Y. Zhou, S. Yang, D. Fan, J. Reilly, H. Zhang, W. Yao, J. Huang, Carbon Quantum Dot/TiO2 Nanohybrids: Efficient Photocatalysts for Hydrogen Generation via Intimate Contact and Efficient Charge Separation, Acs Applied Nano Materials 2(2) (2019) 1027-1032.
[26] X. Yu, R. Liu, G. Zhang, H. Cao, Carbon quantum dots as novel sensitizers for photoelectrochemical solar hydrogen generation and their size-dependent effect, Nanotechnology 24(33) (2013).
[27] M. Feng, Y. Liu, N. Wei, S. Ma, Z. Li, H. Li, S. Chen, J. Liu, D. Wang, Alumina anchored CQDs/TiO2 nanorods by atomic layer deposition for efficient photoelectrochemical water splitting under solar light, Journal of Materials Chemistry a 6(37) (2018) 18293-18303.
[28] J. Bian, C. Huang, L. Wang, T. Hung, W. Daoud, R. Zhang, Carbon Dot Loading and TiO2 Nanorod Length Dependence of Photoelectrochemical Properties in Carbon Dot/TiO2 Nanorod Array Nanocomposites, Acs Applied Materials & Interfaces 6(7) (2014) 4883-4890.
[29] T. Feng, Q. Zeng, S. Lu, M. Yang, S. Tao, Y. Chen, Y. Zhao, B. Yang, Morphological and Interfacial Engineering of Cobalt-Based Electrocatalysts by Carbon Dots for Enhanced Water Splitting, Acs Sustainable Chemistry & Engineering 7(7) (2019) 7047-7057.
[30] S. Xie, H. Su, W. Wei, M. Li, Y. Tong, Z. Mao, Remarkable photoelectrochemical performance of carbon dots sensitized TiO2 under visible light irradiation, Journal of Materials Chemistry a 2(39) (2014) 16365-16368.
[31] X. Xie, Y. Yang, Y. Xiao, X. Huang, Q. Shi, W. Zhang, Enhancement of photoelectrochemical activity of Fe2O3 nanowires decorated with carbon quantum dots, International Journal of Hydrogen Energy 43(14) (2018) 6954-6962.
[32] D. Cammi, K. Zimmermann, R. Gorny, A. Vogt, F. Dissinger, A. Gad, N. Markiewcz, A. Waag, J. Prades, C. Ronning, S. Waldvogel, T. Voss, Enhancement of the Sub-Band-Gap Photoconductivity in ZnO Nanowires through Surface Functionalization with Carbon Nanodots, Journal of Physical Chemistry C 122(3) (2018) 1852-1859.
[33] W. Shi, X. Zhang, J. Brillet, D. Huang, M. Li, M. Wang, Y. Shen, Significant enhancement of the photoelectrochemical activity of WO3 nanoflakes by carbon quantum dots decoration, Carbon 105 (2016) 387-393.
[34] J. Wang, Y. Ng, Y. Lim, G. Ho, Vegetable-extracted carbon dots and their nanocomposites for enhanced photocatalytic H-2 production, Rsc Advances 4(83) (2014) 44117-44123.
[35] L. Wang, X. Wu, S. Guo, M. Han, Y. Zhou, Y. Sun, H. Huang, Y. Liu, Z. Kang, Mesoporous nitrogen, sulfur co-doped carbon dots/CoS hybrid as an efficient electrocatalyst for hydrogen evolution, Journal of Materials Chemistry a 5(6) (2017) 2717-2723.
[36] X. Xu, Z. Bao, G. Zhou, H. Zeng, J. Hu, Enriching Photoelectrons via Three Transition Channels in Amino Conjugated Carbon Quantum Dots to Boost Photocatalytic Hydrogen Generation, Acs Applied Materials & Interfaces 8(22) (2016) 14118-14124.
[37] R. Shi, Z. Li, H. Yu, L. Shang, C. Zhou, G. Waterhouse, L. Wu, T. Zhang, Effect of Nitrogen Doping Level on the Performance of N-Doped Carbon Quantum Dot/TiO2

Composites for Photocatalytic Hydrogen Evolution, Chemsuschem 10(22) (2017) 4650-4656.
[38] L. Sang, L. Lei, J. Lin, H. Ge, Co-sensitization of TiO2 electrode with Eosin Y dye and carbon dots for photoelectrochemical water splitting: The enhanced dye adsorption and the charge transfer route, International Journal of Hydrogen Energy 42(50) (2017) 29686-29693.
[39] L. Vallan, E. Urriolabeitia, F. Ruiperez, J. Matxain, R. Canton-Vitoria, N. Tagmatarchis, A. Benito, W. Maser, Supramolecular-Enhanced Charge Transfer within Entangled Polyamide Chains as the Origin of the Universal Blue Fluorescence of Polymer Carbon Dots, Journal of the American Chemical Society 140(40) (2018) 12862-12869.
[40] L. Vallan, E.P. Urriolabeitia, A.M. Benito, W.K. Maser, A versatile room-temperature method for the preparation of customized fluorescent non-conjugated polymer dots, Polymer 177 (2019) 97-101.
[41] J. Coates, Interpretation of Infrared spectra, a practical approach, in: R.A. Meyers (Ed.), Encyclopedia of Analytical Chemistry, Wiley, Chichester, 2000, pp. 10815-10837.
[42] H. Li, W. Shi, W. Huang, E. Yao, J. Han, Z. Chen, S. Liu, Y. Shen, M. Wang, Y. Yang, Carbon Quantum Dots/TiOx Electron Transport Layer Boosts Efficiency of Planar Heterojunction Perovskite Solar Cells to 19%, Nano Letters 17(4) (2017) 2328-2335.
[43] S. Sidhik, J. Velusamy, E. De la Rosa, S. Perez-Garcia, G. Ramos-Ortiz, T. Lopez-Luke, Role of carbon nanodots in defect passivation and photo-sensitization of mesoscopic-TiO2 for perovskite solar cells, Carbon 146 (2019) 388-398.
[44] H. Bian, Q. Wang, S. Yang, C. Yan, H. Wang, L. Liang, Z. Jin, G. Wang, S. Liu, Nitrogen-doped graphene quantum dots for 80% photoluminescence quantum yield for inorganic -CsPbI3 perovskite solar cells with efficiency beyond 16%, Journal of Materials Chemistry a 7(10) (2019) 5740-5747.
[45] G. Kang, S. Lee, J. Yeo, E. Choi, D. Lee, S. Na, H. Joh, Graphene quantum dots with nitrogen and oxygen derived from simultaneous reaction of solvent as exfoliant and dopant, Chemical Engineering Journal 372 (2019) 624-630.

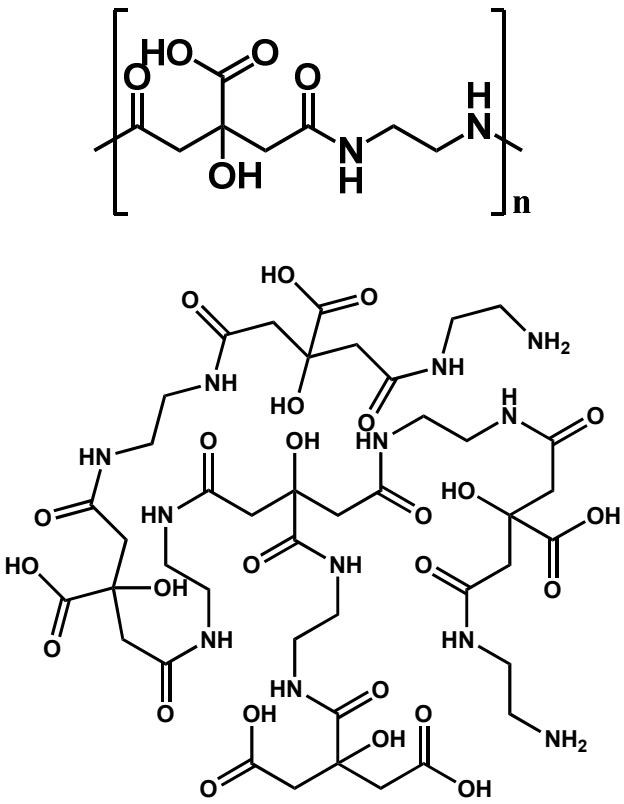

Figure 1. Top) chemical structure of a linear polymer that results from the polycondensation between citric acid and ethylenediamine; bottom) model secondary structure of the polymer MW-CDs.

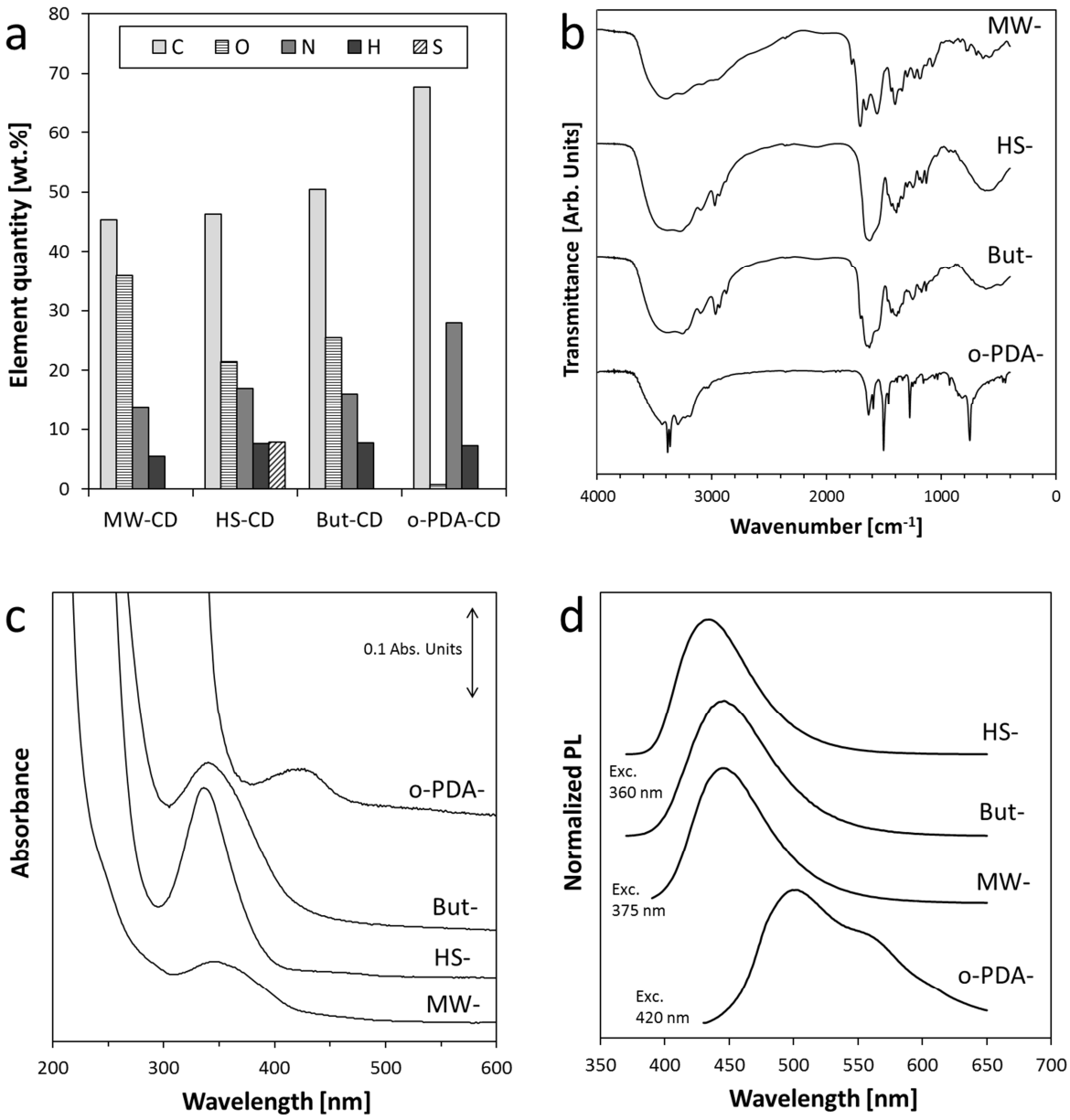

Figure 2. Characterization of the different CD types: a) elemental analysis, b) IR spectra, c) UV-Vis absorbance spectra, and d) PL emission spectra.

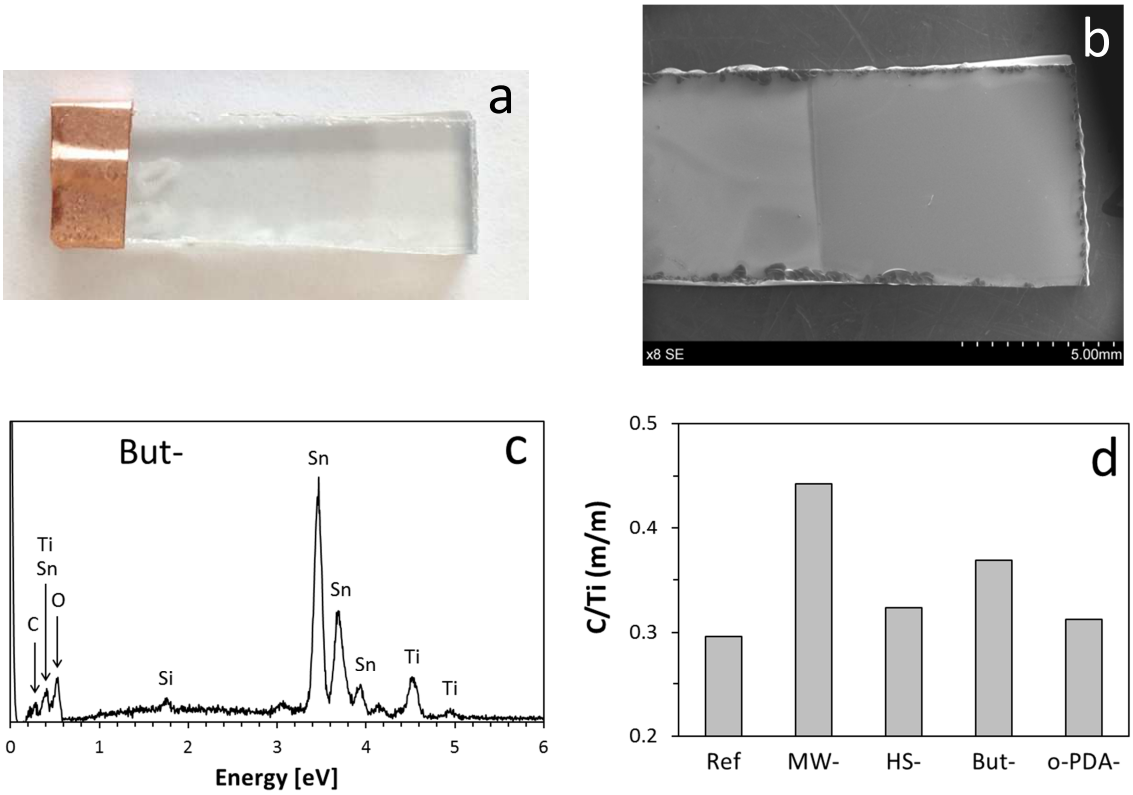

Figure 3. Characterization of c-TiO_2 / m-TiO_2 + CD electrodes by SEM-EDX: a) picture of the electrode, b) image of the electrode by SEM, c) EDX spectrum, and d) C/Ti mass ratio of the reference c-TiO_2 / m-TiO_2 and electrodes with different types of CDs.

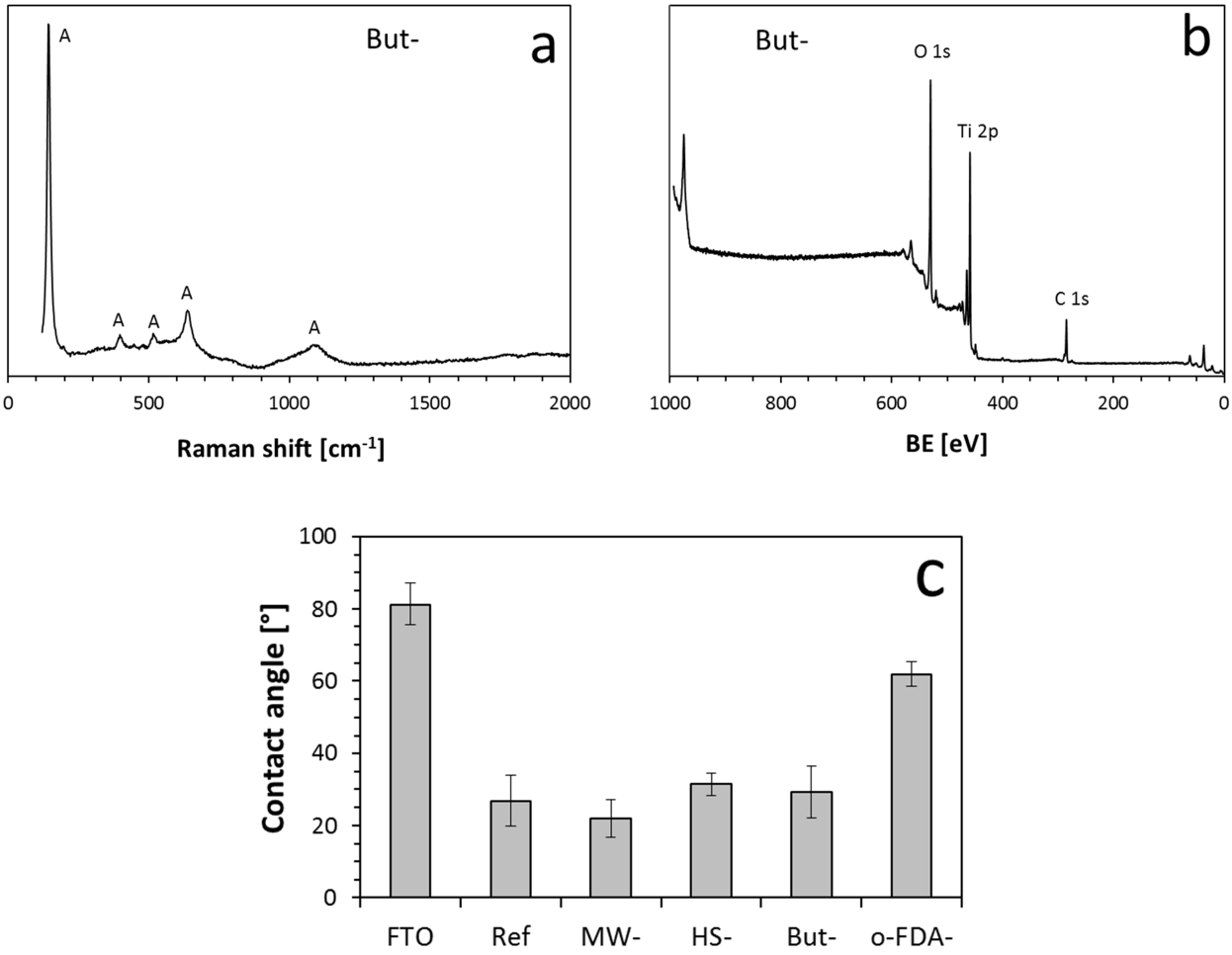

Figure 4. Characterization of c-TiO_2 / m-TiO_2 + CD electrodes: a) Raman, b) XPS, and c) static contact angle measurements with pure water on the reference c-TiO_2 / m-TiO_2 and electrodes with different types of CDs.

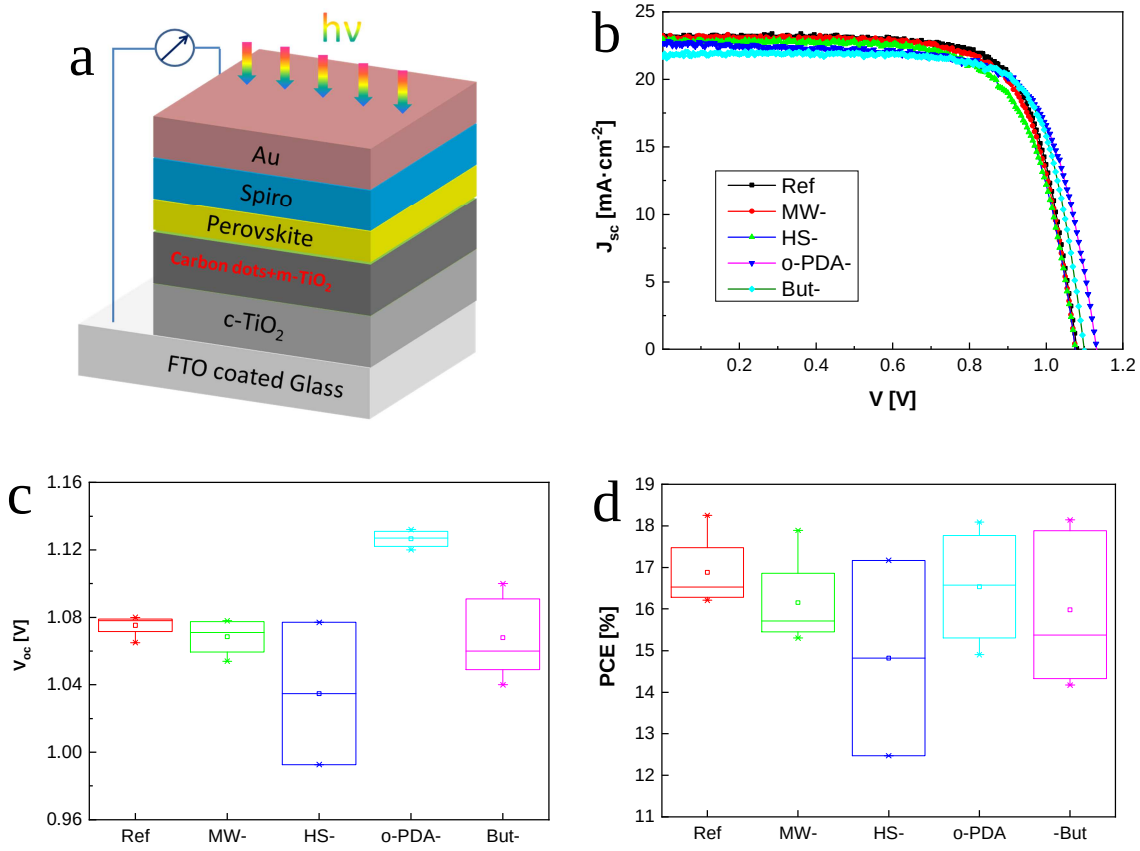

Figure 5. Schematic configuration and characterization of perovskite cells: a) schematic explaining the cell layer components; b) j_{SC} vs. V statistics; c) V_{OC}; and d) PCE statistics for the reference c-TiO_2 / m-TiO_2 and electrodes bearing different functionalized CDs.

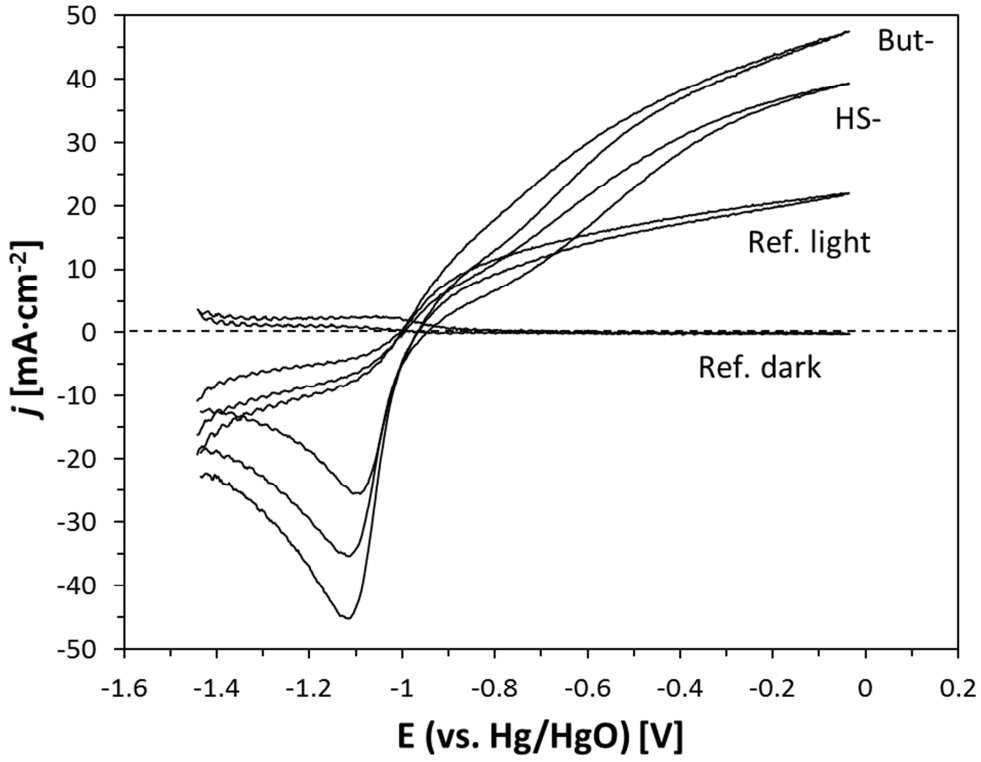

Figure 6. CV analysis of the reference c-TiO_2 / m-TiO_2 electrode (dark and light conditions) and electrodes bearing HS- and But-CDs under irradiation.

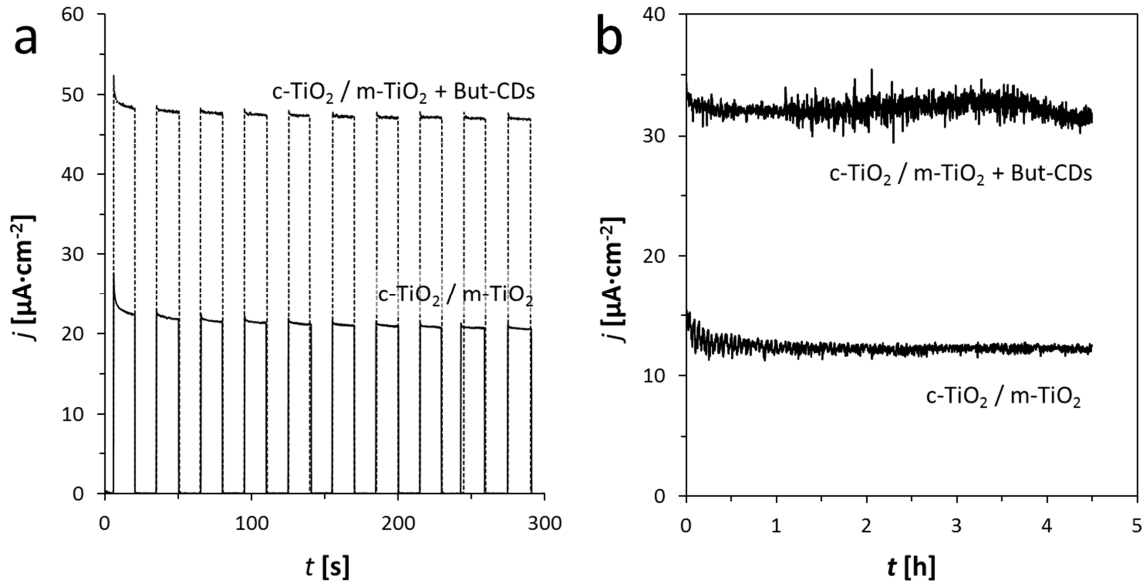

Figure 7. Photocurrent measurements under potentiostatic conditions: a) On/off irradiation at -0.037 V vs. Hg/HgO; b) continuous illumination at -0.280 V vs. Hg/HgO.

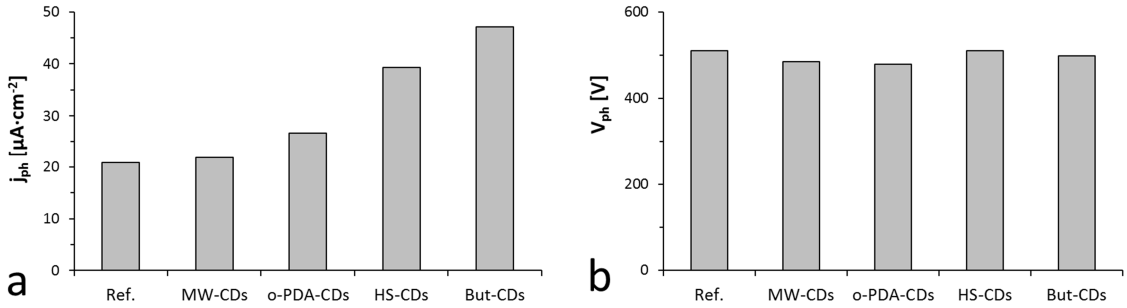

Figure 8. Parameters of PEC water oxidation on the reference c-TiO_2 / m-TiO_2 and electrodes bearing different functionalized CDs: a) potentiostatic photocurrent at -0.037 V vs. Hg/HgO; b) photopotential.

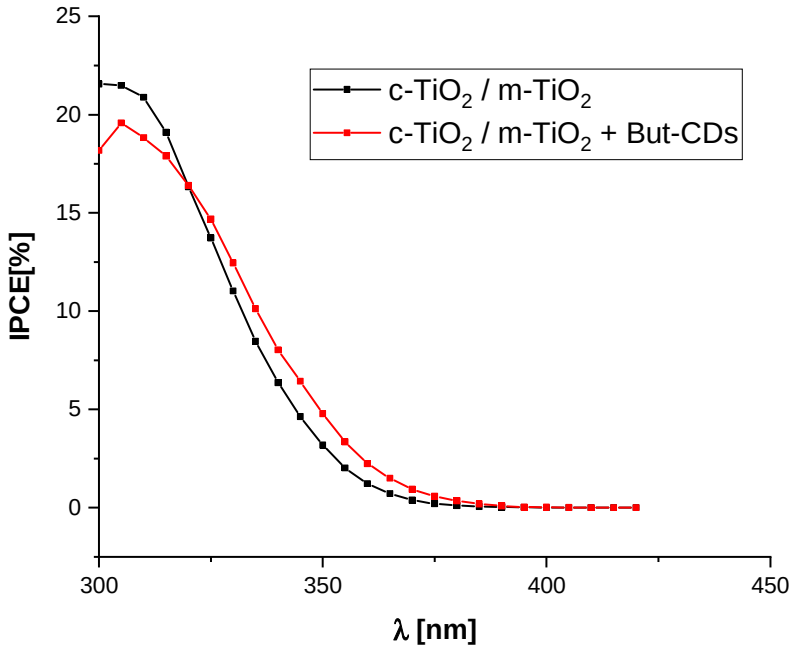

Figure 9. IPCE measurement on the reference c-TiO_2 / m-TiO_2 and the modified c-TiO_2 / m-TiO_2 + But-CDs electrode in 0.1M NaOH at -0.037 V (vs. Hg/HgO).

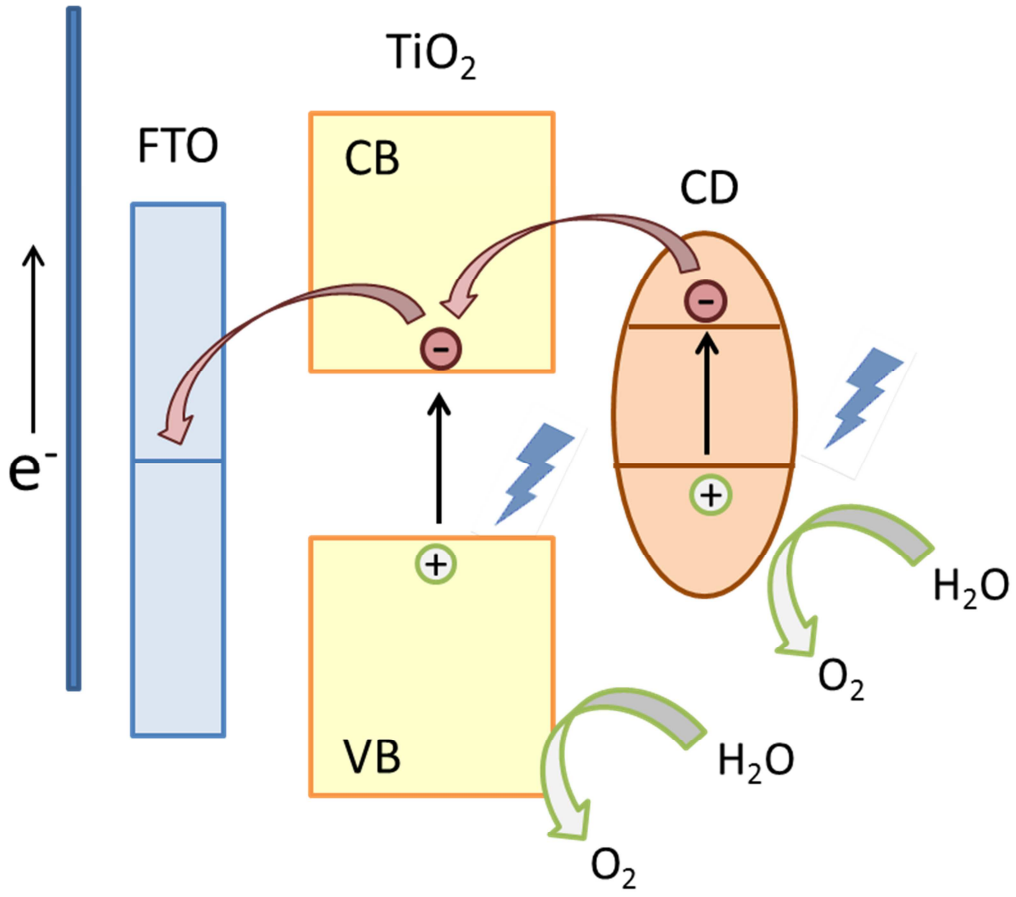

Figure 10. Schematic explaining the mechanism of PEC water oxidation on modified c-TiO_2 / m-TiO_2 + CD electrodes: both the TiO_2 and CDs work as semiconductors; all the photoexcited electrons flow through the TiO_2 layer (CB = conduction band; VB = valence band).